2019

Nonlinear Vector Current Source for theControl of Permanent Magnet SynchronousGenerators in Wave Energy Applications

D. RAMÍREZ, H. MENDONÇA, M. BLANCO, F. MARTÍNEZ

This is an “Accepted article” version of a paper and it is not the “Final published article” version as appearing in IET Renewable Power Generation (Volume: 13, Issue: 13, October 2019).and published on 24 July 2019.

"This is the peer reviewed version of the following article: **Ramirez, D., Mendonça, H., Blanco, M. and Martinez, F. (2019), Non-linear vector current source for the control of permanent magnet synchronous generators in wave energy applications. IET Renewable Power Generation, 13: 2409-2417.** ***which has been published in final form at*** https://doi.org/10.1049/iet-rpg.2019.0122***. This article may be used for non-commercial purposes in accordance with Wiley Terms and Conditions for Use of Self-Archived Versions. This article may not be enhanced, enriched or otherwise transformed into a derivative work, without express permission from Wiley or by statutory rights under applicable legislation. Copyright notices must not be removed, obscured or modified. The article must be linked to Wiley’s version of record on Wiley Online Library and any embedding, framing or otherwise making available the article or pages thereof by third parties from platforms, services and websites other than Wiley Online Library must be prohibited."***

For more information, please consult the WYLEY Post-Publication Policies

How to Cite this article:

Ramirez, D., Mendonça, H., Blanco, M. and Martinez, F. (2019), Non-linear vector current source for the control of permanent magnet synchronous generators in wave energy applications. IET Renewable Power Generation, 13: 2409-2417. https://doi.org/10.1049/iet-rpg.2019.0122

DOI: https://doi.org/10.1049/iet-rpg.2019.0122

IET Research Journals

Research Paper

IET Journals
The Institution of Engineering and Technology

ISSN 1751-8644
doi: 0000000000
www.ietdl.org

Nonlinear Vector Current Source for the Control of Permanent Magnet Synchronous Generators in Wave Energy Applications

D. Ramirez[1] *H. Mendonça*[1] *M. Blanco*[2] *F. Martinez*[3]

[1] *Department of Electrical Engineering, ETSI Industriales, Universidad Politécnica de Madrid, Madrid 28006, Spain*
[2] *CIEMAT, Spain*
[3] *Department of Electronic Technology Department, University of Valladolid, Spain*
** E-mail: dionisio.ramirez@upm.es*

Abstract: A current source with a space-vector hysteresis- band and a constant switching frequency has been designed to be used with surface-mounted permanent magnet synchronous generators. Its fast response makes it very suitable to carry out the precise control necessary in Wave Energy Converters (WEC). These systems are characterized by large variations of speed, torque (or force) and frequency that means that the control has to cope with large variations of voltage and current and also with persistent periods where these variables present low values. The control system takes into account both rotation direction (or displacement direction, when a linear generator is considered) and electrical sequences, something necessary in WEC such as point absorbers. The algorithm was successfully tested in the laboratory using an ad hoc built emulator, that reproduces the behavior of an oscillating water column based WEC. The emulator was built using a similar hardware to those used in equivalent real systems.

1 Introduction

A wave energy converter (WEC) consists of a prime mover, a Power Take-Off (PTO) and a control system, normally based on an electronic converter controlled by a microprocessor. The function of the control system is to drive the PTO so that it operates at its maximum efficiency point under all operating conditions [1–5]. Because of the oscillating nature of the wave, the speed and torque or force provided by the prime mover to the PTO undergoes large and steep fluctuations. Therefore, the control system is required to have a fast response, not delayed by the effect of the numerical integration used in proportional-integral (PI) regulators in traditional vector control of electric machines [6].

The control of a Permanent Magnet Synchronous Generator (PMSG) is usually performed by a Voltage Source Converter (VSC). It works as a voltage source regulated by means of a current feedback to carry out an indirect torque (or force) and field control [7].

Another possibility for a more direct and faster control is to use the electronic converter as a nonlinear current source, although traditional algorithms (bang-bang controllers, etc.) present disadvantages such as non-constant switching frequency and unpredictable harmonic content [8]. However, hysteresis current control of voltage-source converters offers simplicity, lack of tracking errors, independence of load parameter changes, and unmatched transient response in comparison with other techniques. These characteristics make it advisable to adopt this method in all cases where high accuracy and wide bandwidth are required [9, 10] such as the highly irregular (in amplitude and frequency) power profile generated in wave power plants.

Recently, different control strategies for voltage source converters have been introduced such as model based predictive control (MPC). This type of control considers the model of the system, and according to a cost function and the control objectives, chooses the optimal voltage vector [11, 12]. However, this approach presents a high ripple in the control variables, and the switching frequency, similarly to direct torque control (DTC), is variable, although there are alternative strategies to overcome these downsides [13, 14].

Another recent control strategy is the direct power control (DPC). It provides a fast control but presents variable switching frequency and high ripple in the torque and power [11, 12].

Several strategies for fault tolerance [15, 16] have also been developed for double-fed induction generator (DFIG) and PMSG in wind energy and could be applicable to wave energy, reducing the maintenance cost, increasing the productivity and the survival of buoy-based WECs in circumstances where control would be lost, etc.

Specifically for the control of oscillating water column (OWC) power plants, systems designed to control the rotation speed of the DFIGs connected to the turbine have been recently published. For example, an event triggered backstepping controller (ET-BSC) and an event triggered sliding mode controller (ET-SMC) were successfully tested in [17] with the ET-BSC performing better than the ET-SMC. Other system use a maximum power point tracking (MPPT) controller [18] to continuously adjust the speed of the DFIG according to a previously established curve. All of them are intended to avoid the stalling problem associated to Wells turbines, to remove this power output limit.

Complementary controls to the electric generator control have also been proposed to improve the wave power conversion such as controlling the airflow through the throttle valve [19] or by the prediction of the wave elevation inside the chamber of the OWC [20]. In addition, the oscillation of the generated power can be smoothed by adding storage capability [21, 22].

In [23], an OWC power plant emulator (waves, chamber, turbine) is presented, but the dynamic control of the torque generated by the Wells turbine and applied to the PMSG is not addressed and, indeed, the control strategy does not make use of any dynamic equation of the PMSG. Therefore, a simple diode-based rectifier with a DC/DC converter was sufficient. By contrast, the nonlinear vector current source (NLVCS) proposed in this work is based on the dynamic equations of the PMSG and it requires the use of a three-phase converter controlled by a microcontroller. As a result, unlike [23], the hardware setup used in this paper comprises three microcontrollers (instead of two), they are dual core (instead of single core) and they are interconnected over the Internet to keep the synchronization of the beginning and the end of the tests, to share alarms and for monitoring tasks.

In [24] a NLVCS based on the electrical equations of a grid connected three-phase converter is presented. In this simple case, the

© The Institution of Engineering and Technology 2015

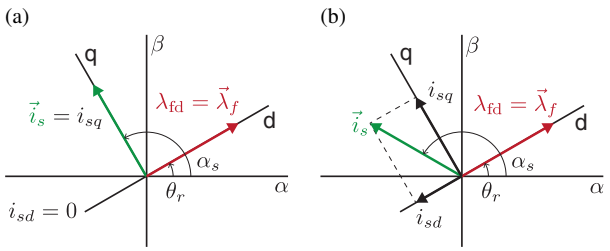

Fig. 1: Torque control.
a Under rated speed at rated voltage.
b Field weakening. Above rated speed at rated voltage.

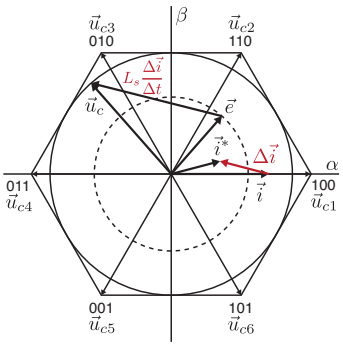

Fig. 2: Calculation of the necessary $\Delta\vec{i}$ and the corresponding $\vec{u}_c$.

frequency and the voltage amplitude are constant and the whole system (inputs and outputs) is electrical. By contrast, in the new strategy presented in this paper, the calculations performed by the NLVCS are based on the dynamic electromechanical equations of the PMSG. Indeed, the objective of this new proposal is to dynamically control the mechanical torque and the magnetic field of the machine from the stator currents. This new NLVCS allows to perform a maximum power point tracking technique, magnetic field weakening, etc. In addition, it is robust to parameter variations in the electrical generator.

To solve the equations in every cycle, the proposed strategy must estimate the emf generated by the generator from the electromechanic equations of the PMSG and measurements. It is important to highlight that, in this application, the electrical quantities present large variations of amplitude and frequency. Also, the operations carried out by the algorithm are different resulting in a constant cycle time that makes its programming on a microcontroller easier. Other features associated to wave energy power plants have been considered within the proposed algorithm such as the overvoltage generated by transient over-speed (prevented by field weakening), code tuning to cope with wide emf and frequency ranges, or related to technical limitations such as the measurement of occasionally extremely low rotation speed and shaft angle, etc.

2 Control Algorithm

The NLVCS control algorithm is based on the space-vector model of the PMSG, comprising an emf source and an inductor in series, and the reference frame is synchronized with the magnetic field axis in order to allow torque and field control of the generator.

On the one hand, the shaft speed is regulated to obtain the maximum electric power from the PTO. Thus, the speed is taken to the maximum efficiency point (according to the power generation) by controlling the load torque, T_e, provided by the PMSG, Fig. 1(a) [7]:

$$T_e = \frac{p}{2}\lambda_{fd} i_{sq} \tag{1}$$

where λ_{fd} is the magnetic field provided by the magnets, p the number of poles and i_{sq} is one of the components of the stator current in a rotating reference frame where the d-axis is aligned with the rotor flux.

In addition, the magnetic field is also controlled. Under normal operating conditions, the field is exclusively provided by the surface-mounted magnets so the reference for i_{sd} is set to zero, Fig. 1(a). Only when, occasionally, the shaft speed exceeds the rated value, field weakening is performed by regulating $i_{sd} < 0$, but keeping it away from the point of irreversible demagnetization, Fig. 1(b).

In order to set the i_{sd} and i_{sq} references for the generator, the value of the electromotive force (emf) vector, $\vec{e}$, must be constantly calculated. It can be done by measuring voltages and currents, and using the electrical machine model [7]:

$$\vec{e} = \vec{u}_c - R_s\vec{i} - L_s\frac{\mathrm{d}\vec{i}}{\mathrm{d}t} \tag{2}$$

expressed in the stationary reference frame, where $\vec{u}_c$ is the converter voltage, and R_s and L_s are, respectively, the generator resistance and inductance.

Nevertheless, as long as the magnetic field is constant in the PMSG ($\lambda_{sd} = \lambda_{fd}$) by keeping $i_{sd} = 0$, the emf can be calculated as follows:

$$|\vec{e}| = \lambda_{sd} \cdot \omega \tag{3}$$

However, in the field weakening region ($i_{sd} < 0$), the total magnetic field has to be calculated as:

$$\lambda_{sd} = L_{sd} \cdot i_{sd} + \lambda_{fd} \tag{4}$$

The magnetic field λ_{fd} can be previously calculated by measuring the voltage and the speed in the unloaded generator. Also, a rotor position measurement is necessary to obtain the vector angle, but it has to be noted that this angle and the shaft speed are available since they are used by the vector control algorithm.

Following the program code sequence, the algorithm first calculates the direction of the space-vector current increment necessary to get the desired current value in the real generator at the end of the next control cycle, as shown in Fig. 2.

Thus, the current increment, $\Delta\vec{i}$, is obtained by comparing the reference current vector, $(i_{\alpha\,\text{ref}}, i_{\beta\,\text{ref}})$, and the measured current vector, (i_α, i_β), both of them expressed in the stationary reference frame:

$$\Delta i_\alpha = i_{\alpha\,\text{ref}} - i_\alpha \tag{5}$$

$$\Delta i_\beta = i_{\beta\,\text{ref}} - i_\beta \tag{6}$$

Next, taking into account the actual value of the emf, $\vec{e}$, the voltage vector to be applied by the inverter, $\vec{u}_c$, in order to get the desired $\Delta\vec{i}$, is calculated as follows (neglecting the term $R_s\vec{i}$):

$$\vec{u}_c \approx L_s\frac{\mathrm{d}\vec{i}}{\mathrm{d}t} + \vec{e} \tag{7}$$

For each current vector location there are four possible current increments, as a function of the sign of its coordinates, so there are four possible solutions for $\vec{u}_c$. Its value is calculated in every microprocessor program cycle by using the PMSG terminals equation (this approximation becomes less accurate as the shaft speed slows down and the emf decreases), Fig. 3.

The maximum voltage vector, $\vec{u}_c$, describes a circumference of radius $R = 0.866 \cdot U_{dc}$. Therefore, the $\vec{u}_c$ to be generated in the next program cycle can be obtained by calculating the intersection between a straight line with the desired slope, $\mathrm{d}\vec{i}/\mathrm{d}t$, and the circumference described by $\vec{u}_c$, Fig. 3.

The algorithm implementation was carried out by studying the solutions in the vertical axis, β, and the location of the vectors $\vec{e}$ and $\Delta\vec{i}$. It can be verified that when $\Delta i_\beta > 0$, the solution for the intersection of the straight line $L_s\mathrm{d}\vec{i}/\mathrm{d}t$ and the circumference described

© The Institution of Engineering and Technology 2015

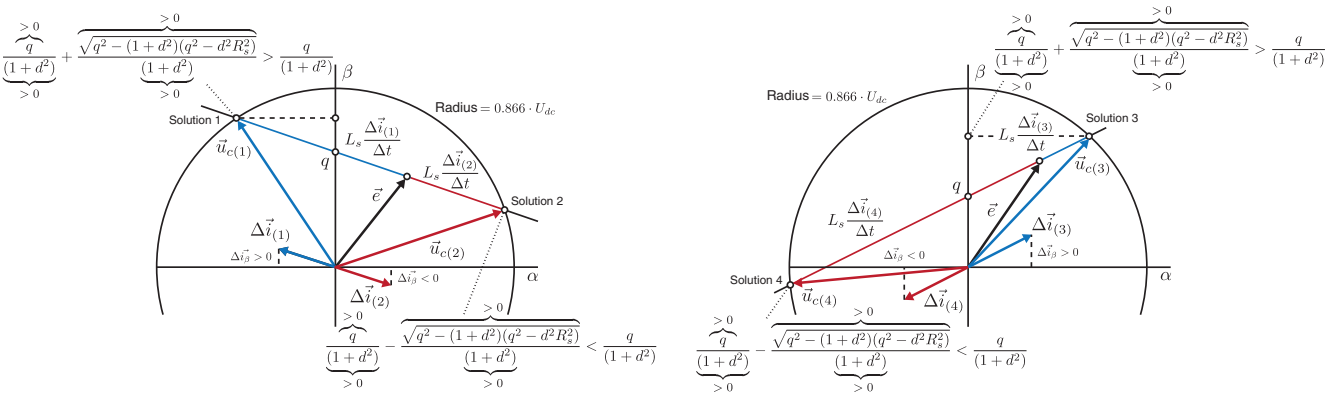

Fig. 3: There are four main possibilities for $\Delta\vec{i}$ in each program cycle.

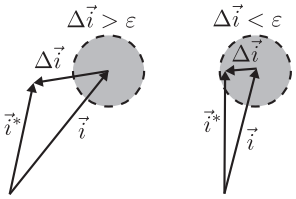

Fig. 4: Space hysteresis area around the current space vector. Two possible cases: $|\Delta\vec{i}| > \varepsilon$ and $|\Delta\vec{i}| < \varepsilon$ in each program cycle.

by the inverter voltage vector is:

$$u_{c\beta} = \frac{q + \sqrt{q^2 - (1+d^2)\cdot(q^2 - d^2R_s^2)}}{1 - d^2} \tag{8}$$

Likewise, when $\Delta i_\beta < 0$, the solution is always:

$$u_{c\beta} = \frac{q - \sqrt{q^2 - (1+d^2)\cdot(q^2 - d^2R_s^2)}}{1 - d^2} \tag{9}$$

where q is the intersection point of the straight line and the vertical axis, d the slope of this line and R the radius of the circumference.

By using this algorithm it is possible to obtain the correct solution by calculating a single square root in each microprocessor cycle, which leads to a considerable computation time saving in the PMSG control (between $2.75\,\mu s$ and $12\,\mu s$ depending on whether a lookup-table or a standard iterative C function is used). In addition, it provides a more constant cycle time, which is an advantage for predicting the total computation time of the control program, something fundamental when choosing the ADC sampling period and the SVM PWM cycle time.

The control system, detailed in Section 4, uses a single P-I regulator to control the rotation speed through the torque (by means of i_{sq}) and it does not need any P-I regulator to control the magnetic field. The typical inner control loops for i_{sd} and i_{sq} have been replaced by a NLVCS.

Note that, by directly imposing the value of the α and β components of the current (or d and q), the need for using the decoupling terms necessary to obtain the corresponding voltages in d and q is eliminated, which makes independent control in both axes easier.

The duty cycle of the PWM within the SVM is not corrected in all the control cycles since it depends on whether the increment of current space vector exceeds a certain space hysteresis area around the tip of the electric current vector in each program cycle, Fig. 4.

The algorithm is able to adapt itself to both electrical sequences, positive and negative, depending on the direction of the speed applied to the electrical generator.

This feature would be necessary, for example, in the case of point absorbers. In some of these systems, the heave oscillating movement of the floating body is directly translated into changes of direction in the generator shaft rotation since they are connected to each other through a mechanism such as rack and pinion. In the cases of a direct drive PTO system, the motion is directly transmitted to the translator of a linear generator [25]. In these two previously mentioned cases, the NLVCS controls the electromagnetic force instead of the electromagnetic torque [4]. Both cases make the voltage to alternate between the positive and negative sequences.

3 Simulation of the NLVCS

In this Section, the proposed algorithm is implemented in Simulink/MATLAB and applied to the direct drive point absorber model presented in [4] and to the OWC power plant model presented in [1, 2, 23, 26] . For the simulations in the following Sections 3.1 and 3.2, a wave data series (WDS) was synthetically generated by using the Pierson-Moskowitz (PM) spectrum [27], with the significant height $H_s = 1$ m and energy period $T_e = 10$ s.

3.1 Direct Drive Point Absorber

The point absorber WEC model is composed of a floating body connected to a linear PMSG by a very stiff rope. Depending on the position of the moving parts, buoy and translator, their motion is coupled or not. This simulation has been carried out in order to verify the effectiveness of the NLVCS under positive and negative sequences generated by the irregular and bidirectional oscillation of the translator velocity. The NLVCS in the current controller block is controlled by using the optimal control proposed in [4], where the impedance seen from the generator terminals must be purely resistive with value R_{op}. Therefore, in this approach, the voltage and current at the generator terminals should be kept in phase by the controller and the NLVCS. The simplified electrical scheme of this WEC model is shown in Fig. 5(a), where the grid-side connection is modeled as a DC source.

For the WDS, the optimal resistance, R_{op}, was set to $2\,\Omega$. The responses of the WEC over time are shown in detail in Fig. 6, between $t = 5$ s and $t = 11$ s. Within this interval, the translator speed direction changes at about $t = 8$ s as well as the corresponding sequence of voltages and currents. It can be seen in Fig. 6(a) that, whichever the translator direction, the NLVCS is able to ensure the correct control operation, where the ratio $u_a/i_{sa} = 2$.

Another simulation is carried on with the same wave profile. However, now R_{op} alternates between 10 and $0.25\,\Omega$ every 0.2 seconds to check its dynamic response under fast and abrupt changes in the control variable R_{op}. Fig. 6b shows the behavior of the voltage and current in phase-a at the terminal generator under this condition. Again, the NLVCS operates correctly and presents a fast dynamic response, reaching the condition u_a/i_{sa} almost instantaneously despite the changes in the direction of the velocity and the rough conditions of the control variable.

© The Institution of Engineering and Technology 2015

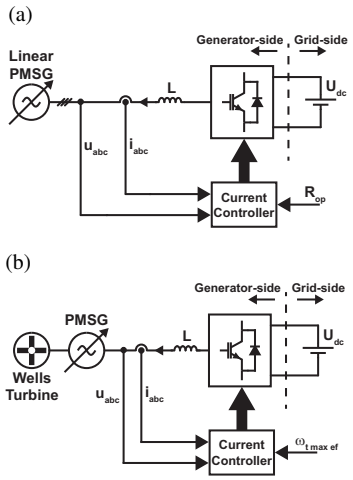

Fig. 5: Simplified schemes of WECs.
a Direct drive point absorber [4].
b OWC power plant [23].

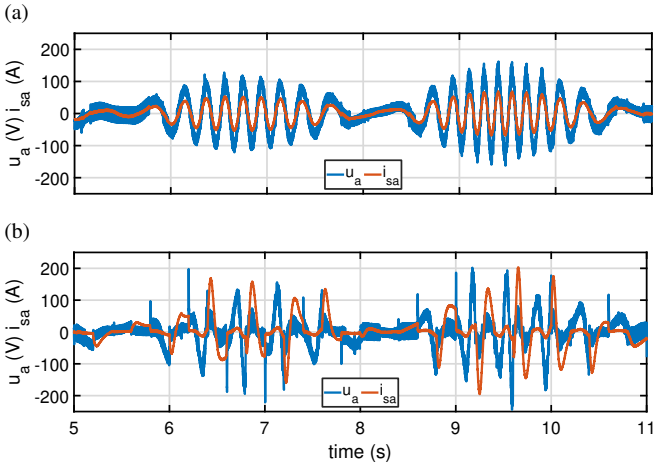

Fig. 6: Simulation of the direct drive WEC in [4] with the nonlinear current source in the current controller.
a Voltage and current in phase a at the terminal generator for $R_{op} = 2\,\Omega$.
b Voltage and current in phase a at the terminal generator for R_{op} changing between 10 and $0.25\,\Omega$ every 0.2 seconds.

Once verified the effectiveness of the proposed NLVSC algorithm, it has been compared with a conventional current controller implemented with PI [8]. For this, a regular wave profile has been used and R_{op} has been changed in 2 s time intervals and, consequently, the reference current too. Fig. 7 shows the current at the linear PMSG terminals in two different time windows. Both cases demonstrate the fast response of the NLVSC, where the generated current follows the current reference. On the other hand, the PI-based controller presents a slower dynamic response and it takes a time to establish the current. In addition, as can be seen in Fig. 7, the difference between the reference current and the one generated by the PI-based controller can reach up to 12 A.

3.2 OWC

The OWC is a WEC whose energy chain conversion is divided into three steps: first, the mechanical energy of the waves to the pneumatic energy in the OWC chamber; second, pneumatic to mechanical through the Wells turbine; and, finally, mechanical to electrical in the PMSG.

3.2.1 Chamber Model: The detailed modelling of the chamber in an OWC device, from the fluid mechanics point of view, gives rise

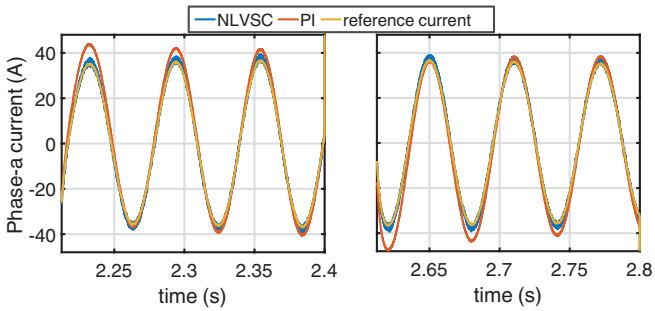

Fig. 7: Performance of the current controller implemented with the proposed NLVSC and the conventional PI.

to complex mathematical models. However, the hardware implementation of the emulator imposes some limits because of the hardware and cycle time constraints, so it is necessary to reach a compromise between the level of detail of the model and the capabilities of the hardware on which this model is running. As, from the point of view of the electric generation, a high degree of detail is not necessary, it was decided to use a simplified model.

The restrictions considered in the chamber model were:

- The air column inside the chamber was considered incompressible, meaning that air losses have been neglected.
- The height of the water surface inside the chamber was considered equal to the height reached by the wave. This assumption is reasonable when the wavelength of the incident ocean wave is much bigger than the dimensions of the water surface in motion inside the chamber.

Also, this means that the transfer function between the incident wave and the chamber oscillations, the memory effects related to wave radiation and the effects of the force related to the pressure variation on the oscillating water mass are neglected. This makes the two systems, oscillating water column and PTO, decoupled. As a consequence, the hydrodynamics inside the chamber is not fully described but, from the electrical point of view, the power delivered to the grid does not lose the multifrequency spectrum of the waves.

The OWC device equations include a simplified chamber model where the vertical speed is calculated as:

$$V_x = \left(\frac{A_c}{A_d}\right) \cdot \frac{\partial h_c}{\partial t} \tag{10}$$

whose variables are defined in Table 1.

3.2.2 Wells Turbine Model: The Wells turbine is represented through the torque obtained from the air flow. Fig. 8 shows, in solid line, the characteristic curve of a generic turbine model [28] where, in turn, the flow coefficient, Φ, is a function of the air flow through the turbine:

$$\Phi = \frac{V_x}{r_t \cdot \omega_t} \tag{11}$$

The torque, T_t, produced by the Wells turbine is calculated through the torque coefficient, C_t, represented in Fig. 8, which depends on the characteristic curve of each particular turbine, described by:

$$T_t = C_t \cdot K \cdot r_t \cdot \left[V_x^2 + (r_t \cdot \omega_t)^2\right] \tag{12}$$

where K is a constant of the turbine.

Due to the PMSG, voltage and frequency are variable (as in Section 3.1), but, in this case, the Wells turbine makes the PMSG operate only in direct sequence. Fig. 5(b) shows the electrical simplified scheme of this OWC.

© The Institution of Engineering and Technology 2015

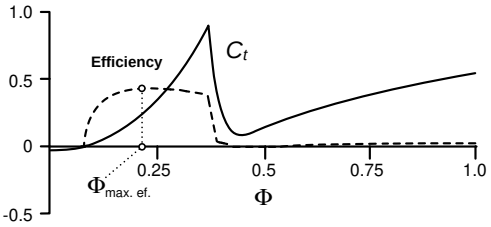

Fig. 8: Generic C_t and efficiency as a function of the flow coefficient, used to model the Wells turbine.

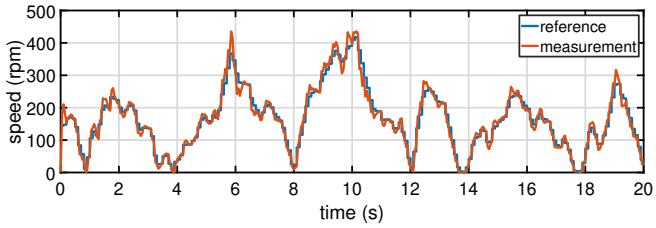

Fig. 9: OWC simulation. Maximum efficiency speed reference (blue) and measured speed (red).

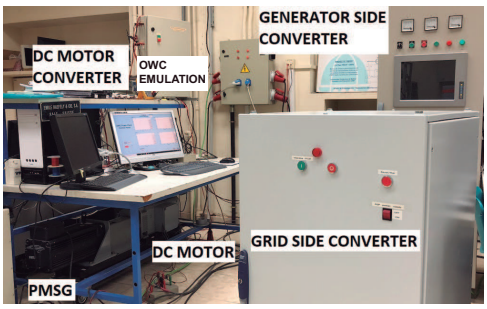

Fig. 10: Test bench for OWC applications.

Note that this system is very similar to the one in Fig. 5(a). Apart from the energy chain conversion, the difference is the control strategy to maximize the power extraction. In this case, the one presented in [1, 2] is implemented, where the control variable is the angular velocity of the rotor, ω_t, that must be set to achieve the maximum turbine efficiency in the efficiency curve [29] in Fig. 8 through the corresponding flow coefficient, $\Phi_{\text{max ef}}$. In effect, by substituting $\Phi_{\text{max ef}}$, V_x (measured in a real power plant or calculated from the waves in the emulator) and the turbine radius, r_t, in Eq. (11), the microcontroller obtains the maximum efficiency speed in every program cycle. Fig. 12(a) summarizes the implementation of the OWC in DSP-1.

The good performances of the NLVCS are confirmed by the result obtained since it shows an actual PMSG shaft speed very close to the reference speed over the 4 minutes simulated for this WDS. Fig. 9 shows this result for 20 s for better visualization.

4 Hardware Emulator. Description

In order to test the current source behavior in real conditions, a customized emulator was used (Fig. 10). It comprises one separately excited DC Motor (to reproduce the self-rectifying turbine torque), one three-phase surface mounted permanent magnet synchronous generator, one three-phase step-up transformer for grid connection, three electronic converters and a control system composed by 3 dual core microprocessors, Fig. 11. Among the self-rectifying turbines used in OWC systems, a Wells Turbine was chosen for the emulation due to it being one of the most commonly studied and used technology.

From the functional point of view, the simulator consists of three main systems:

- OWC simulator (system 1): it comprises the wave and the OWC chamber simulation as well as the Wells turbine model. They were programmed using C language and the torque generated by the turbine was reproduced by using a DC motor driven by a DC/DC converter. The control of this system was implemented in the dual core DSP 1 [24].
- Power Take-Off (system 2): it is composed by a PMSG and the back-to-back VSC necessary for the control of the generator. The nonlinear current source control of this system was implemented in the dual core DSP 2.
- Grid connection (system 3): it consists of a three-phase inverter and its vector control system, programmed in the third microprocessor, the dual core DSP 3.

Microcontrollers specifically designed for power plants and electric drive control were chosen, and they feature internet connection capabilities for Smart Grid integration. All DSPs are Texas Instruments (TI) F28M35x Concerto, consisting of two very different cores: one ARM Cortex M3 and one TI C28. This architecture was chosen because it allows independent communication tasks (with the user or other DSPs) and control tasks.

Internally, the communication between the cores was carried out through a shared RAM memory and a message-based protocol. As they feature internet connection, the communication between the DSPs was carried out using the laboratory WiFi, but the user can choose between USB or WiFi communication. In the latter case, control or monitoring can be performed even from outside the Lab. Each control system has its specifically designed user interface, developed using Matlab GUI or LabView.

The equations of the simplified models of the OWC chamber and the Wells turbine programmed in the DSP 1 were the same as used in [1, 23], whose variables are summarized in Table 1. These models and the control system are shown as a block diagram in Fig. 12(a), where the torque to be reproduced is calculated by means of Eq. (12).

Fig. 12(b) shows the control block diagram of the nonlinear current source implemented and tested in system 2 over the PMSG. The current component i_{sq} controls the generator torque, T_e, (and therefore the rotation speed) and the component i_{sd}, the magnetic field. The ω_t required to achieve the maximum turbine efficiency was imposed by system 2, which calculates this speed in each program cycle by Eq. (11) with $\Phi_{\text{max ef}}$. Normally, i_{sd} is kept to zero in order to not modify the magnetic field provided by the permanent magnets, but if the shaft speed exceeds the rated speed, a field weakening is carried out limited by the irreversible demagnetization point. Also, a typical vector control for grid connection was implemented, in system 3, Fig. 12(c).

Since a hardware technology (DSP, inverters, generator, etc.) representative of a real power plant has been used, the emulator built in the laboratory has turned out useful, not only to obtain experimental results in order to verify the properties of the control algorithm, but also to investigate the particularities and technological limitations associated with wave energy power plants. These particularities might be a consequence of the technologies used, either the type of generator (PMSG, etc.), measurement limitations (wide range of speeds, occasionally extremely low speeds, etc.), or others that need to be taken into account by modifying the control program (transient over-speed, wide emf and frequency ranges, occasional extremely low and durable emf, etc.).

5 Experimental Results

Next, the experimental results obtained from the hardware setup described in the previous section under several different tests are presented.

© The Institution of Engineering and Technology 2015

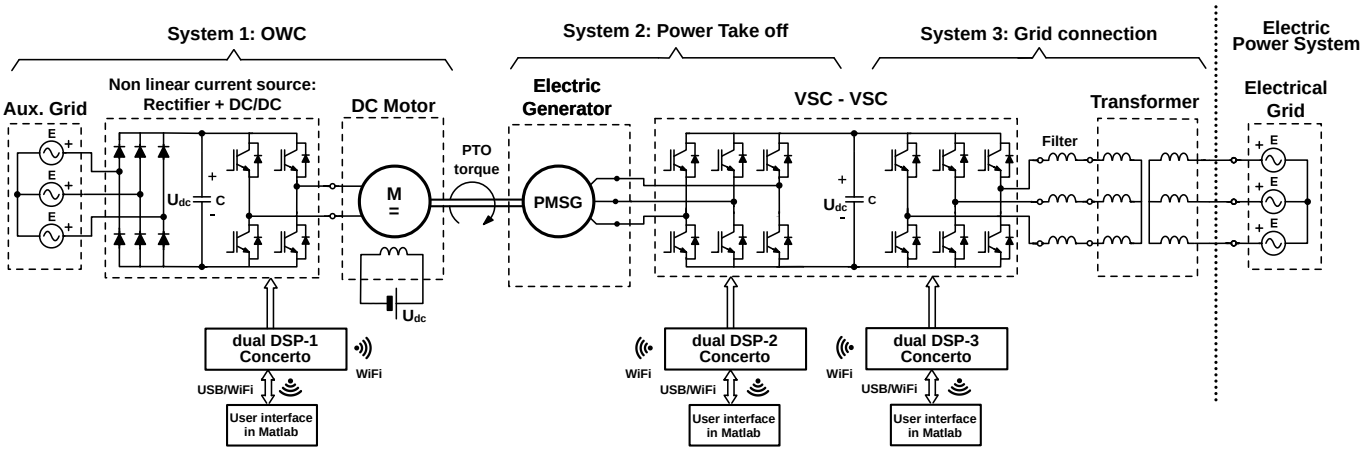

Fig. 11: Electrical scheme of the emulator implemented in the lab. Note the back-to-back VSC.

5.1 Steady State Test

In the first test, the nonlinear current source was tested for constant PMSG rotation speed (470 rpm). Several values of i_{sd} and i_{sq} were imposed to the generator using the current source, as it is shown in the following figures. Fig. 13 shows the shape of the stator currents when the nonlinear current source feeds the PMSG.

5.2 Dynamic Response Test

Fig. 14 shows the step response of i_{sq} (torque) when it changes from -2 A to -5 A and from -2 A to -10 A whereas i_{sd} (magnetic field) is set to 0 . The results show the fast dynamic provided by the NLVCS to control the torque by means of i_{sq}.

5.3 Dynamic Response Test in the Field Weakening Region

In a wave energy power plant, the irregular wave might lead the shaft speed to values greater than the rated one. In this situation, the emf can overpass the insulation rated value of the windings, destroying them. To avoid it, it would be necessary to partially demagnetize the PMSG setting the i_{sd} to a negative value. In order to prevent this problem, the OWC chamber must also feature a pressure relief valve (which is a common practice). Fig. 15 shows a demagnetizing test carried out with the generator rotating at 650 rpm, i_{sq} set to -6 A and step current i_{sd} of 0 and -2 A. The result shows the fast dynamic provided by the NLVCS to weaken the magnetic field of the PMSG.

5.4 Maximum Efficiency Speed Test

In this test, the ability of the current source to impose the maximum efficiency speed on the generator was tested over four minutes, using 2400 wave samples. The control system needs to know the rotor position in order to calculate the magnetic field position. There are several ways to work this out: using a resolver, an encoder, a sliding mode observer, etc. In this test, an encoder featuring index signal to signal the completion of every revolution was used.

Fig. 16 shows the measured magnetic field position, used to determine the d-q reference frame position. It can be seen something that characterize the wave energy applications: large changes in the speed caused by the irregular wave. This fact introduces an extra difficulty for the control since there are periods presenting very slow rotation speed, even around zero, that can change to a fast rotation speed. These changes imply angular position and speed calculation algorithm must adapt quickly to avoid introducing any error. Depending on the sea state, the wave can experience persistent periods of low turbine and generator rotation speed may happen, making difficult to keep the synchronization with the magnets field as well as to control the power source when the emf is close to zero.

Due to the large speed variations experienced by generators deployed in wave energy, the emf presents a wide range of frequency and amplitude values. These large variations are a key point in the nonlinear current source operation since $\Delta\vec{i}$ is, ultimately, generated by the difference between $\vec{e}$ and the voltage generated by the inverter $\vec{u}_c$. Fig. 17 shows the $\vec{e}$ measured by the microprocessor, expressed by means of its two components in the static reference frame. Note the large amplitude and frequency variations .

The PMSG stator current shows large variations, Fig. 18. This is a consequence of the irregular torque applied to the PMSG shaft by the Wells turbine (the emulator in this case) and, ultimately, of the irregular wave, leading to a variable rotation speed. The DSP-2 task is to take the PMSG shaft speed to the maximum efficiency point in every moment and, to achieve that, the NLVCS has to impose the needed current value in every moment. Due to the highly variable speed (and emf), the stator current has to be variable as well. Also, the nonlinear operation of the current source used leads to an irregular shape in the waveform.

The q-component of the PMSG stator current in the magnetic field reference frame, i_{sq}, provides a measurement of the generator torque since they are proportional. Fig. 19 shows that this component was always negative throughout the test since the generator torque was also negative (opposed to the motor torque provided by the Wells turbine). The i_{sq} waveform presents large variations due to two reasons: the irregular wave leads to an irregular Wells turbine torque but, also, the nonlinear operation of the current source generates nonsinusoidal currents that lead to a non-smooth waveform.

The d-component of the stator current, i_{sd}, represents the electromagnetic field generated by the stator currents and windings. Since no overexcitation or field weakening was required in this test, it was kept to zero in order to avoid extra iron losses or demagnetizing the permanent magnets in the rotor. Fig. 19 shows the i_{sd} waveform, kept around zero during the test.

Fig. 20 shows how the actual PMSG shaft rotation speed, measured by the DSP-2 using an encoder (red) and the maximum efficiency speed (blue), were continuously superimposed, which proves that the nonlinear current source provided an excellent PTO control.

5.5 Robustness Test

The NLVCS needs to estimate the emf in every program cycle. In this test, the constant that relates the rotor speed and the emf, Eq. (3), has been changed by 40%. Even so, the result shows a rotor speed very close to the reference, Fig. 21. The value of the stator resistance is not taken into account in the NLVCS but it could become important at low speeds, when the voltage drop in R_s is comparable to the voltage supply. However, the results of the test have shown that, even a very slow speeds, the actual speed is close to the reference. The stator inductance value has no effect on the NLVCS since the voltage vector is calculated from the derivative of the stator current Eq. (7).

© The Institution of Engineering and Technology 2015

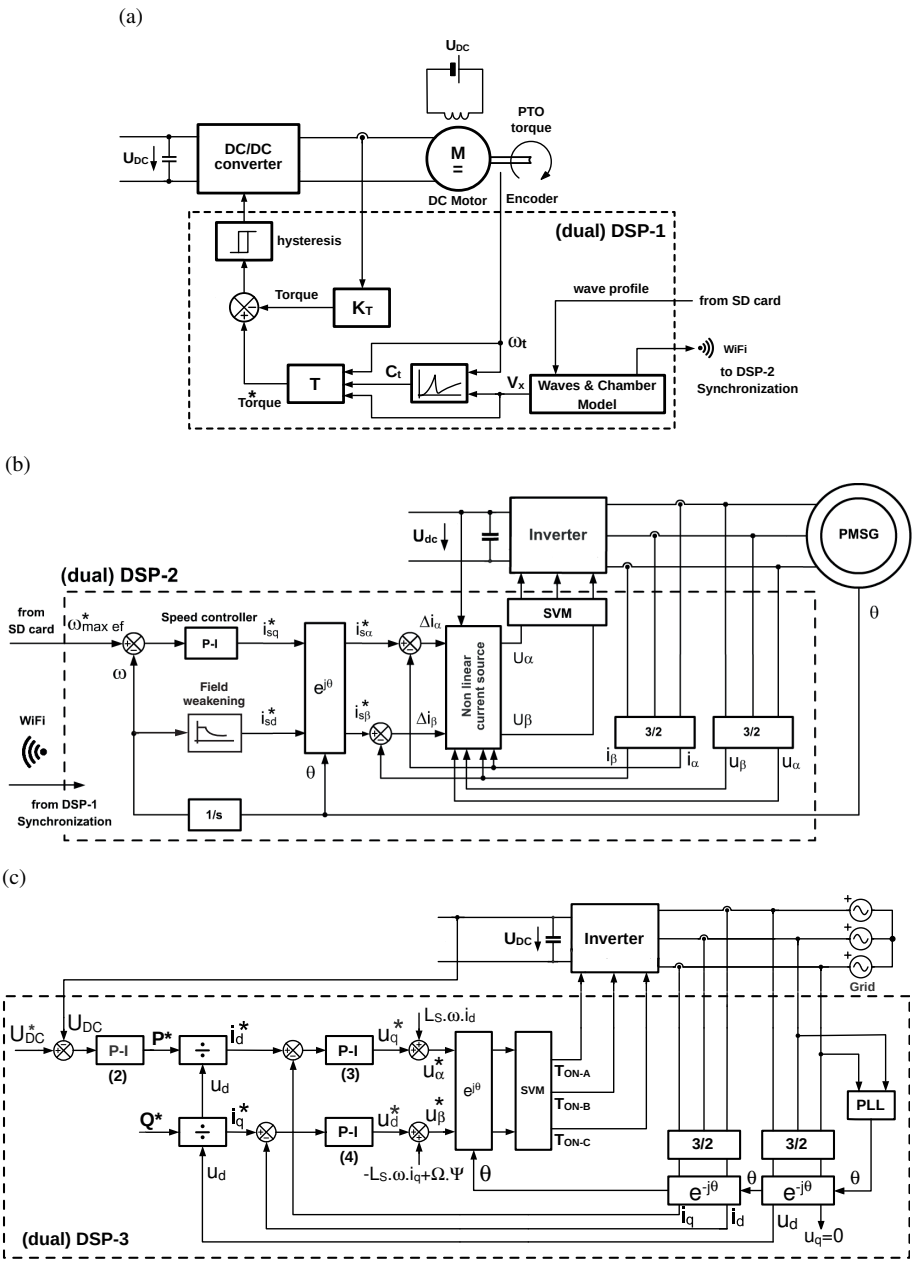

Fig. 12: Control block diagram implemented in the dual-core DSPs.
a DSP-1: OWC system.
b DSP-2: PTO system.
c DSP-3: Grid connection system.

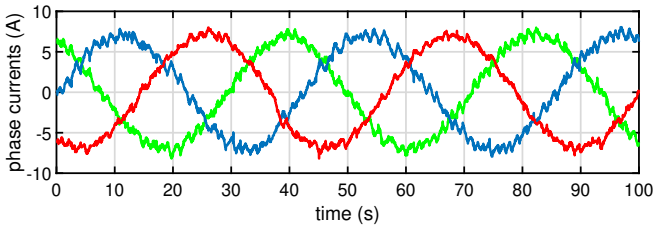

Fig. 13: Three phase current in the PMSG stator in steady state test when $i_{sq} = -10$ A and $i_{sd} = 0$ A, acquired using a Tektronix TPS 2024 oscilloscope.

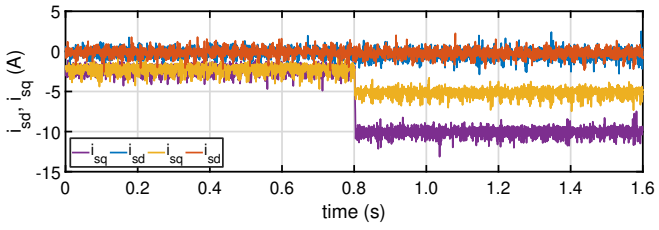

Fig. 14: Evolution of i_{sd} (magnetic field) and i_{sq} (torque) during the step response tests.

5.6 *Computation Time*

Fig. 21(a) shows the NLVCS computation time of the earlier version of the NLVCS presented in [24] for the case of a grid connection and Fig. 21(b) shows the computation time of the current version, presented in this paper for a PMSG control. The new implementation of the algorithm saves 6.6 μs (28% or 39% respect to the old and the new computation time respectively) and assures a constant computation time because only one square root is calculated each cycle,

© The Institution of Engineering and Technology 2015

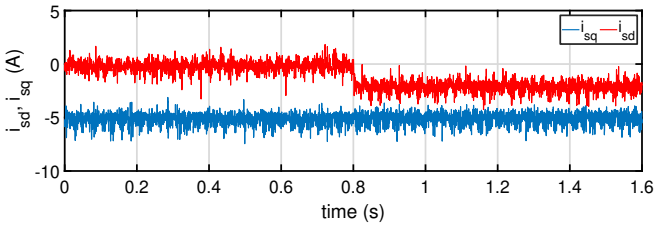

Fig. 15: Evolution of i_{sd} and i_{sq} during the field weakening test.

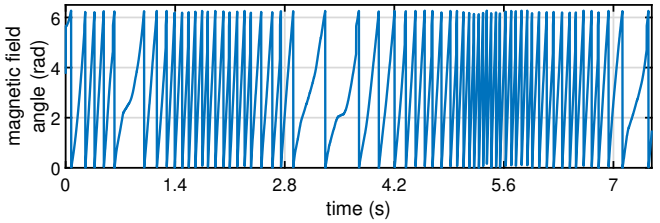

Fig. 16: Magnetic field angle during the starting.

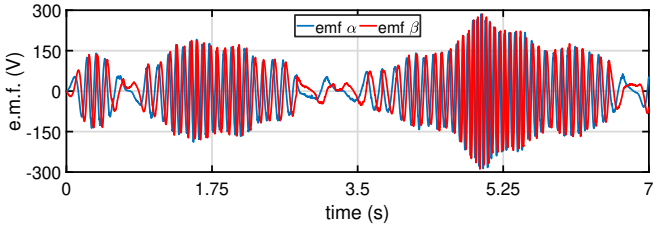

Fig. 17: Emf components in the static reference frame $\alpha\beta$.

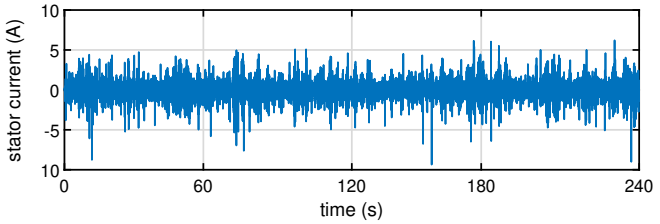

Fig. 18: Stator current measured throughout the test.

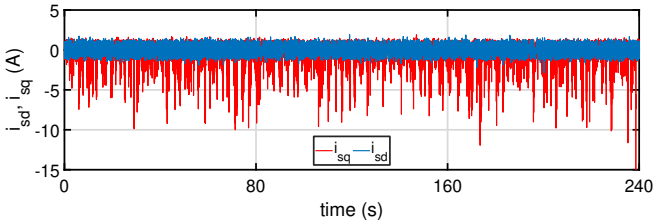

Fig. 19: dq currents throughout the test. i_{sq} and i_{sd} set to zero.

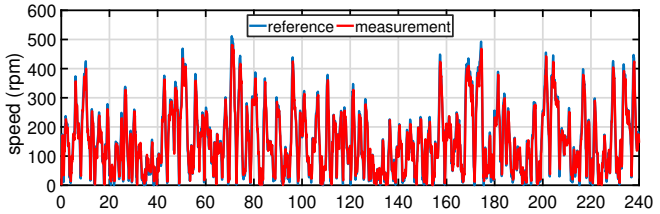

Fig. 20: In blue, maximum efficiency speed reference. In red, actual shaft speed measured using an encoder.

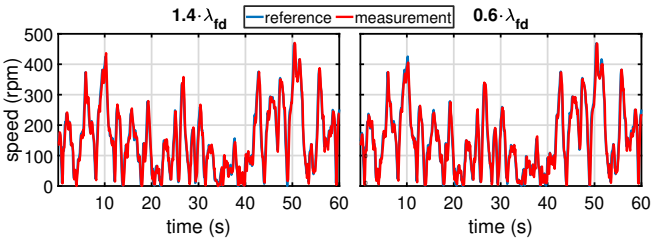

Fig. 21: Maximum efficiency speed reference (blue) and measured speed (red) for λ_{fd} variations of $\pm 40\%$.

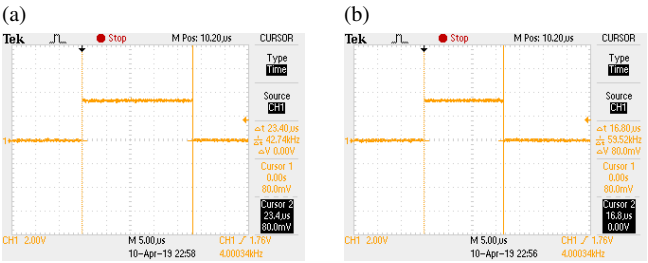

Fig. 22: NLVCS computation time.
a Worst case of the version presented in [24].
b Constant time of the new version presented in this paper.

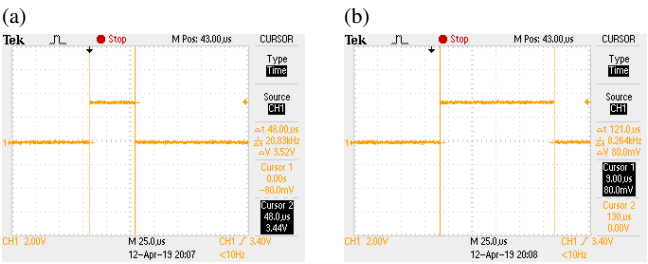

Fig. 23: MPC computation time.
a Minimum computation time.
b Maximum computation time.

whereas in the earlier version the MCU had to calculate one or two depending on whether a certain condition was satisfied. This aspect, a constant computing time, is very important for the programmer since can organize the time spent by each control task better.

For comparison, other advanced and very effective technique, a model predictive control (MPC) for PMSG, has been implemented in the same MCU, obtaining the results shown in Fig. 23. In the MPC case, the computing time is not constant since it depends on whether the algorithm has to make corrections or not after the first iteration. It spends between 48 μs and around 130 μs which means that the programmer has to reserve around 130 μs in the program cycle for the worst case (although the MPC provides the duration times of the modulation which saves the time necessary to compute the SVM, 16.4 μs). In consequence, it can be said that the proposed NLVCS presents a low computing time when compared with other advanced techniques.

It should be noted that these computation times are only approximate since they largely depend on the level of optimization selected in the compilation, the use of optimized or standard functions to calculate the square root, the CPU used, etc.

6 Conclusion

A control system that allows the use of a VSC and the associated space vector modulator as a nonlinear current source to control a PMSG has been developed and tested in a wave energy application.

© The Institution of Engineering and Technology 2015

The cycle time of the current source algorithm is constant, and thus predictable, which makes programming easier in a microprocessor. Also, the algorithm works in both shaft rotation directions and with both generator electrical sequences. A custom hardware emulator was built comprising a PMSG, three electronic converters and six microprocessors, all of them representative of state-of-the-art technology in this type of application. The fast response of the nonlinear current source turned out to be very suitable to impose the torque and magnetic field references in wave energy applications. This is even more relevant if it is considered that in these applications the rotation speed experiences large variations that must be controlled in order to impose the maximum efficiency speed on the PTO. The current source allows to instantly oppose the necessary load torque (by means of the PMSG) to the PTO (Wells turbine) torque. In the event that the shaft rotation speed exceeds the rated value due to an occasional strong wave, the nonlinear current source allows to carry out a field-weakening of the permanent magnet generator in order to avoid possible damages caused by an overvoltage in the windings or in the DC bus. Finally, the algorithm has exhibited great robustness against changes in PMSG parameters.

7 Acknowledgments

This work was supported in part by CAPES, Coordination for the Improvement of Higher Level Personnel (Brazil) under Grant BEX-9376135.

8 References

1 Amundarain, M., Alberdi, M., Garrido, A.J., Garrido, I.: 'Modeling and simulation of wave energy generation plants: Output power control', *IEEE Transactions on Industrial Electronics*, 2011, **58**, (1), pp. 105–117
2 Alberdi, M., Amundarain, M., Garrido, A., Garrido, I., Casquero, O., De la Sen, M.: 'Complementary control of oscillating water column-based wave energy conversion plants to improve the instantaneous power output', *IEEE Transactions on Energy Conversion*, 2011, **26**, (4), pp. 1021–1032
3 Bacelli, G., Ringwood, J.V.: 'Numerical optimal control of wave energy converters', *IEEE Transactions on Sustainable Energy*, 2015, **6**, (2), pp. 294–302
4 Mendonça, H., Martinez, S.: 'A resistance emulation approach to optimize the wave energy harvesting for a direct drive point absorber', *IEEE Transactions on Sustainable Energy*, 2016, **7**, (1), pp. 3–11
5 Anderlini, E., Forehand, D.I., Stansell, P., Xiao, Q., Abusara, M.: 'Control of a point absorber using reinforcement learning', *IEEE Transactions on Sustainable Energy*, 2016, **7**, (4), pp. 1681–1690
6 Lekka, A., Turner, M.C., Menon, P.P.: 'Anti-windup for a class of partially linearisable non-linear systems with application to wave energy converter control', *IET Control Theory & Applications*, 2016, **10**, (18), pp. 2403–2414
7 Novotny, D.W., Lipo, T.A.: 'Vector control and dynamics of AC drives'. vol. 41. (Oxford science publications, 1996)
8 Kazmierkowski, M.P., Malesani, L.: 'Current control techniques for three-phase voltage-source pwm converters: A survey', *IEEE Transactions on industrial electronics*, 1998, **45**, (5), pp. 691–703
9 Malesani, L., Mattavelli, P., Tomasin, P.: 'Improved constant-frequency hysteresis current control of vsi inverters with simple feedforward bandwidth prediction', *IEEE Transactions on Industry Applications*, 1997, **33**, pp. 1194–1202
10 Bhuthukuri, R., Updhyay, P.: 'Review of linear and nonlinear current control techniques for pwm three-phase vsc converters', *International Journal of Engineering Research & Technology*, 2018, **7**, (2)
11 Morel, F., Lin.Shi, X., Rétif, J.M., Allard, B., Buttay, C.: 'A comparative study of predictive current control schemes for a permanent magnet synchronous machine drive', *IEEE Transactions on Industrial Electronics*, 2009, **56**, (7), pp. 2715–2728
12 Zhang, Z., Rodríguez, J., Kennel, R.: 'Advanced control strategies for direct-drive pmsg wind turbine systems: Direct predictive torque control approaches', *CPSS Transactions on Power Electronics and Applications*, 2017, **2**, (3), pp. 217–225
13 Landsmann, P., Kennel, R.: 'Saliency-based sensorless predictive torque control with reduced torque ripple', *IEEE Transactions on Power Electronics*, 2012, **27**, (10), pp. 4311–4320
14 Zhang, Y., Xie, W., Li, Z., Zhang, Y.: 'Model predictive direct power control of a PWM rectifier with duty cycle optimization', *IEEE transactions on power electronics*, 2013, **28**, (11), pp. 5343–5351
15 Cecati, C., Di.Tommaso, A.O., Genduso, F., Miceli, R., Galluzzo, G.R.: 'Comprehensive modeling and experimental testing of fault detection and management of a nonredundant fault-tolerant VSI', *IEEE Transactions on Industrial Electronics*, 2015, **62**, (6), pp. 3945–3954
16 Zhou, D., Zhao, J., Liu, Y.: 'Predictive torque control scheme for three-phase four-switch inverter-fed induction motor drives with DC-link voltages offset suppression', *IEEE Transactions on Power Electronics*, 2015, **30**, (6), pp. 3309–3318
17 Mishra, S.K., Purwar, S., Kishor, N.: 'Event triggered nonlinear control of OWC ocean wave energy plant', *IEEE Transactions on Sustainable Energy*, 2018,
18 Lekube, J., Garrido, A.J., Garrido, I.: 'Rotational speed optimization in oscillating water column wave power plants based on maximum power point tracking.', *IEEE Trans Automation Science and Engineering*, 2017, **14**, (2), pp. 681–691
19 M'zoughi, F., Bouallègue, S., Garrido, A.J., Garrido, I., Ayadi, M.: 'Stalling-free control strategies for oscillating-water-column-based wave power generation plants', *IEEE Trans Energy Convers*, 2017,
20 Paparella, F., Monk, K., Winands, V., Lopes, M., Conley, D., Ringwood, J.V.: 'Upwave and autoregressive methods for short-term wave forecasting for an oscillating water column', *IEEE Transactions on Sustainable Energy*, 2015, **6**, (1), pp. 171–178
21 Lafoz, M., Blanco, M., Beloqui, L., Navarro, G., Moreno.Torres, P.: 'Dimensioning methodology for energy storage devices and wave energy converters supplying isolated loads', *IET Renewable Power Generation*, 2016, **10**, (10), pp. 1468–1476
22 Villalba, I., Blanco, M., Pérez.Díaz, J.I., Fernández, D., Díaz, F., Lafoz, M.: 'Wave farms grid code compliance in isolated small power systems', *IET Renewable Power Generation*, 2018, **13**, (1), pp. 171–179
23 Ramirez, D., Bartolome, J.P., Martinez, S., Herrero, L.C., Blanco, M.: 'Emulation of an owc ocean energy plant with pmsg and irregular wave model', *IEEE Transactions on Sustainable Energy*, 2015, **6**, (4), pp. 1515–1523
24 Ramirez, D., Martinez, S., Carrero, C., Platero, C.A.: 'Improvements in the grid connection of renewable generators with full power converters', *Renewable Energy*, 2012, **43**, pp. 90–100
25 Vining, J., Lipo, T., Venkataramanan, G. 'Experimental evaluation of a doubly-fed linear generator for ocean wave energy applications'. In: Energy Conversion Congress and Exposition (ECCE), 2011 IEEE. (IEEE, 2011. pp. 4115–4122
26 Garrido, A.J., Garrido, I., Amundarain, M., Alberdi, M., De la Sen, M.: 'Sliding-mode control of wave power generation plants', *IEEE Transactions on Industry Applications*, 2012, **48**, (6), pp. 2372–2381
27 Moskowitz, L., Pierson, W.J., Mehr, E. 'Wave spectra estimated from wave records obtained by the OWS weather explorer and the OWS weather reporter'. (U. S. Naval Oceanographic Office, New York Univ., 1962. 63-5
28 Setoguchi, T., Takao, M.: 'Current status of self rectifying air turbines for wave energy conversion', *Energy conversion and management*, 2006, **47**, (15-16), pp. 2382–2396
29 Jayashankar, V., Anand, S., Geetha, T., Santhakumar, S., Kumar, V.J., Ravindran, M., et al.: 'A twin unidirectional impulse turbine topology for owc based wave energy plants', *Renewable energy*, 2009, **34**, (3), pp. 692–698

9 Appendices

Table 1 Turbine model parameters.

T_t	Shaft torque (N·m)	r_t	Turbine radius (m)
Φ	Flow coefficient (nondimensional)	V_x	Air speed in duct (m/s)
C_t	Torque coefficient (nondimensional)	ω_t	Angular velocity of rotor system (rad/s)
K	Constant of the turbine (kg/m)		

Table 2 DC motor and AC generator

DC motor		PMSG	
P_N	7.8 kW	P_N	8.7 kW
U_N	400 V	U_N	400 V
n_N	1092 rpm	n_N	1000 rpm
K_T	3.1	K_T	6.5

Table 3 Wells turbine

Maximum efficiency flux $\Phi_{\text{max ef}} = 0.17$	Maximum C_T before stall	for $\Phi = 0.311$
	Air density	$\rho = 1.2$ kg/m^3
	Height of the blades	$b = 0.045$ m
	Blade chord length	$l = 0.090$ m
	Number of turbine blades	$n = 8$

© The Institution of Engineering and Technology 2015